Exohedral M–C_{60} and M_2–C_{60} (M = Pt, Pd) systems as tunable-gap building blocks for nanoarchitecture and nanocatalysis

Burak Özdamar, Mauro Boero, Carlo Massobrio, Delphine Felder-Flesch, and Sébastien Le Roux

Citation: The Journal of Chemical Physics **143**, 114308 (2015); doi: 10.1063/1.4930264
View online: https://doi.org/10.1063/1.4930264
View Table of Contents: http://aip.scitation.org/toc/jcp/143/11
Published by the American Institute of Physics

Exohedral M–C_{60} and M_2–C_{60} (M = Pt, Pd) systems as tunable-gap building blocks for nanoarchitecture and nanocatalysis

Burak Özdamar, Mauro Boero,[a] Carlo Massobrio, Delphine Felder-Flesch, and Sébastien Le Roux[b]
Institut de Physique et Chimie des Matériaux de Strasbourg, University of Strasbourg and CNRS, UMR 7504, 23 Rue du Loess, BP43, F-67034 Strasbourg, France

(Received 7 July 2015; accepted 26 August 2015; published online 18 September 2015)

Transition metal–fullerenes complexes with metal atoms bound on the external surface of C_{60} are promising building blocks for next-generation fuel cells and catalysts. Yet, at variance with endohedral M@C_{60}, they have received a limited attention. By resorting to first principles simulations, we elucidate structural and electronic properties for the Pd–C_{60}, Pt–C_{60}, PtPd–C_{60}, Pd_2–C_{60}, and Pt_2–C_{60} complexes. The most stable structures feature the metal atom located above a high electron density site, namely, the π bond between two adjacent hexagons (π-66 bond). When two metal atoms are added, the most stable configuration is those in which metal atoms still stand on π-66 bonds but tends to clusterize. The electronic structure, rationalized in terms of localized Wannier functions, provides a clear picture of the underlying interactions responsible for the stability or instability of the complexes, showing a strict relationship between structure and electronic gap. [http://dx.doi.org/10.1063/1.4930264]

I. INTRODUCTION

The design of innovative, green, renewable, and sustainable energy sources has become a worldwide priority in fundamental and applied research. In this global scenario, hydrogen storage and delivery play a prominent role because of two major issues: (i) its production appears to be a clean process promoted by a relatively simple electrocatalysis and (ii) its application in fuel cells results in the production of environmentally friendly water, along with heat and electricity. From the standpoint of energetics, this process has a yield close to 75%, hence higher than a common diesel engine. Coming to the hydrogen storage and production, promising candidates are the Proton Exchange Membrane Fuel Cells (PEMFCs), because of their high capacity and wide range of applications.[1] A general PEMFC is composed of two compartments separated by an ion conducting membrane and designed to convert chemical energy into electric energy. The oxidation of the propellant at the anode and the reduction of the comburant at the cathode produce electricity, heat, and chemical byproducts. At variance with traditional batteries, the PEMFC is an open system, hence propellant and comburant must be continuously supplied. In such a scenario, the design of the catalytic support appears to be a key issue in the development of PEMFC. Using nanoparticles deposited on carbon black aggregates is an efficient way to realize nanostructures with an optimal surface/volume ratio. So far, a lot of efforts have been dedicated to graphene-based systems.[2,3] Yet, fullerenes are likely to disclose a wider variety of possibilities and assembly patterns because of their intrinsic curvature and controlled size.[4,5]

We recently focused on the improvement of the stability of the catalytic support in PEMFC by exploring the possibility of using Buckminster fullerene C_{60} molecule as support to the metallic catalyst. Metallo-fullerene complexes where the metal atoms are coordinated on the external surface of the fullerene cage, termed exohedral metallo-fullerenes, have received much less attention than endohedral M@C_{60} (M = metal) systems[6–9] and doped fullerenes obtained by C replacement with foreign atoms.[10–12] Fullerenes have been the target of studies aimed at encapsulating atoms for a long time. The purpose is to use fullerene cages as a mean to transport and deliver dopants because of their high resistance to external chemical attacks and their thermodynamic stability. Carbon structures like nano-cages and nanotubes being way less sensitive to corrosion than carbon black, it can be inferred that C_{60} could be a good candidate to replace it as well. Moreover, one can link transition metals, such as platinum and palladium, to C_{60} using coordination bonds to create metallo-fullerenes.[13,14]

It is worth pointing out that the first transmission electron microscopy (TEM) observation of Pt–C_{60}[15] has shown that clustering of fullerene molecules and formation of platinum nano-particles can be achieved under controlled conditions. Nonetheless, the interpretation of these experimental observations is elusive, mainly because the strong coupling of different physical and chemical phenomena involved.

In view of the inadequacy of classical force fields to describe systems composed of C_{60} interacting with metallic atoms,[16–18] we rely on first principles simulations within the density functional theory (DFT) framework.[19] This allows to account for both structural and electronic properties, the latter being the major issue in PEMFCs. Specifically, we present a systematic study of fullerenes in interaction with Pt and Pd atoms aimed at identifying the stable structures, resulting from

[a]Electronic address: mauro.boero@ipcms.unistra.fr
[b]Electronic address: sebastien.leroux@ipcms.unistra.fr

specific locations of the metal atoms and their number (one or two) on the external surface of the C_{60}. The geometrical information is supported by a thorough analysis of the local bonding and electronic structure modifications in terms of maximally localized Wannier functions and centers.

II. THEORETICAL MODEL AND COMPUTATIONAL METHODS

Concerning the M-C_{60} (M = Pt, Pd) complexes, a first set of simulations was performed on systems containing $N = 61$ atoms: 60 C and 1 metal atom, either Pt or Pd. After finding the most stable M–C_{60} conformation, a second set of simulations was performed on systems of $N = 62$ atoms: 60 C and 2 metal atoms, either two Pt, two Pd, or a Pd–Pt pair.

The electronic structure was described in the DFT framework with the generalized gradient approximation (GGA) due to Becke (B) for the exchange energy and Lee, Yang, and Parr (LYP) for the correlation energy.[20,21] This specific choice for the description of the exchange-correlation part is supported by the rich literature on the subject.[22,23] For completeness, a comparison with the Perdew-Burke-Ernzerhof (PBE) functional is provided in the first paragraph of the supplementary material. Valence electrons were treated explicitly, in conjunction with norm conserving pseudopotentials of the Trouiller-Martins type to account for core-valence interactions.[24] The wavefunctions were expanded at the Γ point of the supercell on a plane wave (PW) basis set with an energy cutoff $E_c = 100$ Ry. All calculations were performed in simulations cells of side $L = 15$ Å beyond which PWs were damped according to the Barnett-Landman scheme[25] for isolated systems. This allows to get rid of spurious effects induced by periodic boundary conditions generally adopted in PWs approaches. Semi-empirical van der Waals interactions according to the Grimme formulation[27] were included to cope with the possible occurrence of weak metal–fullerene dispersion interactions.[26]

The geometry of each system was fully optimized in two different ways, first by relaxing the structure via direct inversion in the iterative subspace[28] and then by performing damped molecular dynamics.[29] In all dynamical simulations, the Car-Parrinello[30,31] method (CPMD) was adopted for a self-consistent evolution of both the electronic and ionic degrees of freedom. A fictitious electron mass of 500 a.u. (i.e., in units of $m_e a_0^2$, where m_e is the electron mass and a_0 is the Bohr radius) and a time step of $\Delta t = 0.12$ fs are selected to integrate the equations of motion.

The electronic structure of the metal-fullerenes complexes is first inspected by exploiting the Kohn-Sham (KS) states. Then, the information on the bonding is refined in terms of the maximally localized Wannier functions.[32,33] According to a standard procedure, the Wannier functions $w_n(\mathbf{r})$, along with their centers and spreads, are obtained via a unitary transformation *on the fly* of the Kohn-Sham orbitals $\psi_i(\mathbf{r})$. More precisely, among all the possible unitary transformation, the one that minimizes the spread

$$\Omega = \sum_n \left(\langle w_n | \mathbf{r}^2 | w_n \rangle - \langle w_n | \mathbf{r} | w_n \rangle^2 \right) \quad (1)$$

is selected. The Wannier states represent an unbiased method for partitioning the charge density. Hence, the bonding information is summarized by four numbers, the center of the orbital,

$$x_n = -\frac{L}{2\pi} \Im m \log \langle w_n | \exp(-i2\pi \cdot x/L) | w_n \rangle \quad (2)$$

with similar expressions along the other two cartesian directions, and its related spread. Here, L is the length of the simulation cell along the x direction. The analysis of the Wannier function centers (WFCs) with respect to the nuclear positions allows gaining insight into the chemical bonding involved in a wealth of systems such as water,[34] amorphous silicon,[35] fullerenes,[36] and complex electronic structure evolutions involving formation and breaking of chemical bonds.[37,38]

III. ONE METAL ATOM BOUND TO THE FULLERENE

A. Initial configurations

Previous models of fullerene-metal complexes[39,40] were used to construct the initial structures for the present study. The reliability of these models was extensively benchmarked towards experiments and former calculations.[41,42] Thus, five different initial configurations were prepared, differing in the position of the metal atom on the surface of the C_{60}, as summarized in Fig. 1. More precisely, the metal atom is initially placed: (a) on top of a π bond between two adjacent six-carbon rings (π-66 hereafter), (b) on top of a σ bond between a six-carbon ring and a five-carbon pentagon (σ-65 hereafter), (c) on top of the center of an hexagonal ring, (d) on top of the center of a pentagonal ring, and (e) on top of a C atom of the fullerene cage.

These configurations are comprehensive of all the possible symmetries on the C_{60}. For each one of them, full structural optimizations[43] were carried until residual forces were smaller than $\times 10^{-4}$ Hartree/bohr for both metal atoms (M = Pt or Pd). At the end of each optimization cycle, a damped molecular dynamics[29] was performed to further assess the stability of the various structures on the potential energy surface.

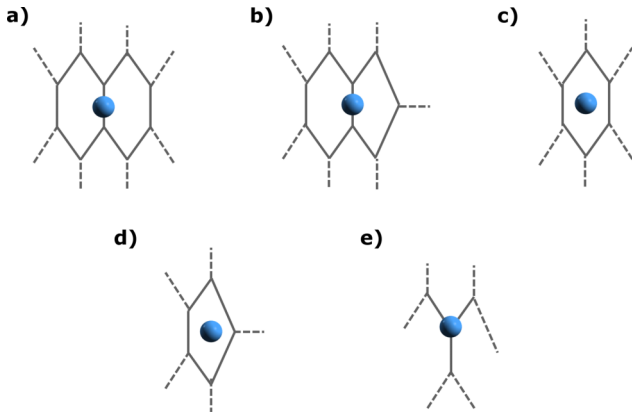

FIG. 1. Schematic representation of the initial configurations used in our simulations. The labels from (a) to (e) refer to the position of the metal atom (Pt or Pd, blue spheres) on the fullerene.

TABLE I. Initial and final M–C_{60} (M = Pt, Pd) configurations and relative energy differences (ΔE) between the final stable structures for each system. ΔE is in eV.

	Pt		Pd	
Initial	Final	ΔE (eV)	Final	ΔE (eV)
a	a	0.0	a	0.0
b	b	0.47	b	0.21
c	a	0.0	a	0.0
d	b	0.47	b	0.21
e	a	0.0	a	0.0

B. Structural properties

The stability of the various configurations are summarized in Table I in terms of relative total energies. In that table, the effects of the damped molecular dynamics become evident by comparing the first and second columns, referring to initial and the final configurations, respectively.

For both metal atoms, only configurations (a) and (b) represent stable states of the fullerene–metal complex. In both cases, the metal atom stands on top of a C–C bond between either two hexagons (π-66) or an hexagon and a pentagon (σ-65). These configurations remain stable also after CPMD simulations lasting about 1.5–2.0 ps and, as such, can be retained as the only two realizable stable complexes. Yet, an energy difference between the two positions of the metal atoms exists. More precisely, the (a) π-66 complex is the most stable minimum for both cases, whereas the (b) σ-65 complex is located above this minimum at 0.47 eV (Pt) and 0.21 eV (Pd). At the equilibrium, the distances of the metal atoms from the two carbon atoms of the C–C bond at the interface of two hexagons (a) or one hexagon and one pentagon (b) are listed in Table II, with the labels of the C atoms corresponding to the ones shown in Fig. 2.

The fact that the σ-65 configuration is less stable than the π-66 is confirmed by a short dynamical run of about 1.5–2.0 ps. One observes a mean square displacements of the metal atoms larger than 3.0 Å ^{2}/s, promoting a departure of the metal atom from the center of the σ-65 C–C bond toward a more favorable stabilization on a nearby π-66 site. Despite the existence of a most stable π-66 configuration, the σ-65 complex has to be retained as a possible alternative equilibrium site for the metal–fullerene complex (see Fig. 2).

C. Electronic properties

Coming to the electronic structure of the stable metal-fullerene complexes, a first feature that can be noticed is a reduction of the energy gap with respect to the pristine C_{60}.

TABLE II. Equilibrium M–C distances, for the configurations (a) and (b). Distances are in Å.

Configurations	C atom	$d_{Pt–C}$	$d_{Pd–C}$
a	C_1	2.03	2.15
a	C_2	2.03	2.15
b	C_3	2.04	2.19
b	C_4	2.04	2.19

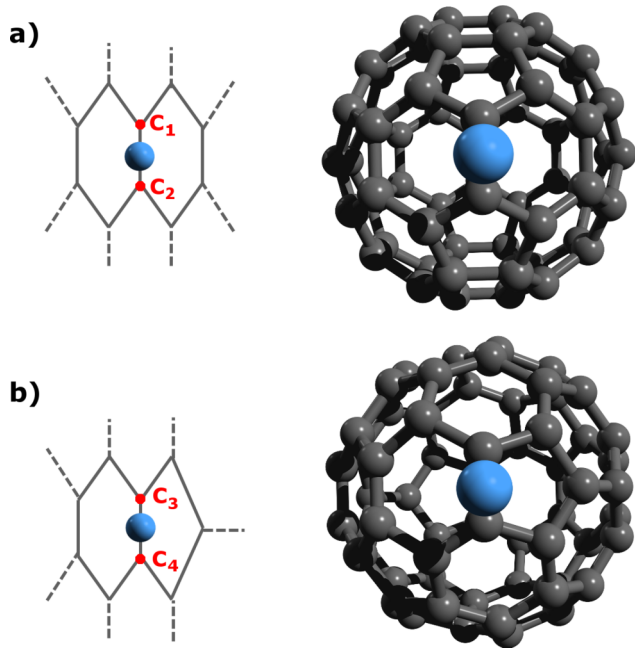

FIG. 2. Schematic (left) and 3D representations (right) of the M–C_{60} complexes for the most stable structures ((a) - π-66) and ((b) - σ-65).

Indeed, an isolated fullerene, according to Becke-Lee-Yang-Parr (BLYP)-based DFT calculations,[44] has a highest occupied molecular orbital (HOMO) possessing a h_u character and a lowest occupied one (LUMO) with a triply degenerate t_{1u} character. They are separated by an energy gap of 1.66 eV. Our calculations show that the presence of a metal atom on a π-66 site is responsible for a decrease in the gap, which reduces to 1.24 eV for Pt and 1.12 eV for Pd. We can also anticipate that the inclusion of additional metal atoms induces a further decrease in the gap to 0.46, 0.56, and 0.84 eV for the complexes Pt_2–C_{60}, PtPd–C_{60}, and Pd_2–C_{60}, respectively. For each complex, we seek for the electronic state best reproducing the HOMO of the isolated fullerene. These states are then aligned to our reference level, i.e., the HOMO of the bare fullerene (Fig. 3). We can remark that the gap shrinking is due

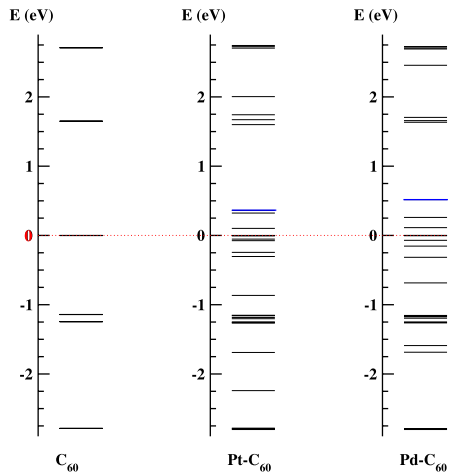

FIG. 3. Kohn-Sham energy levels for the M–C_{60} (M = Pt, Pd) systems compared to the isolated fullerene. The left panel refers to the bare C_{60}, whereas the central and right panels refer to the Pd–C_{60} and the Pt–C_{60} systems, respectively.

to the contribution of orbitals belonging to the metallic atoms, namely, $5d^9 6s^1$ for Pt and $4d^{10}$ for Pd. These levels are located above the h_u HOMO of the C_{60} and become the new HOMO states of the complex M–C_{60}.

The empty or half-filled *s*-orbitals of metal atoms are prone to accept electrons from a general donor in the vicinity. As a result of this donation, existing chemical bonds involved in the process weaken and elongate. Such a mechanism not only facilitates the back-donation of *d*-electrons of the metal atom to the π^* bond of the carbon but also results in a decrease of the band gap.[45] This can explain the inverse relationship between the bond length and the HOMO-LUMO energy difference of the final metallo-fullerene complexes. Thus, it can be inferred that the bond length of M–C increases with the decreasing of the band gap.

For most stable configuration (a), an insight into the nature of the electronic states is provided by the projection of the Kohn-Sham wavefunctions onto atomic orbitals centered on the atoms of interest. Specifically, for our case, the most interesting states are the ones in proximity of the energy gap, being also the ones mostly affected by the formation of M–C (M = Pt, Pd) bonds. For the sake of clarity, we limit the discussion to the case of Pt–C_{60} only, as sketched in Fig. 4. A first feature to be noticed[46] is the arising of typical transition metal-like e_g states in the spectrum of the system. More precisely, the HOMO and HOMO-1 states of the Pt–C_{60} complex are basically pure d_{z^2} and $d_{x^2-y^2}$, respectively, with minor contributions on top of second-neighbor C atoms of the fullerene. Worthy of note is the presence of small amplitudes on top of the two C atoms forming the π-66 bond. Nonetheless, these two e_g states are almost entirely due to 5*d* Pt (or 4*d* for Pd) atomic orbitals of the transition metal bound to the C_{60}. Conversely, the LUMO and LUMO+1 states feature amplitudes dispersed on most of the C atoms of the fullerene (t_{1u} and t_{1g}-like[44]), with negligible contribution of the transition metal atom.

The maximally localized WFCs provide an insightful complementary information about the nature of the chemical bonds. Their associated spreads allow to identify how many electronic states — and to which extent — contribute to the metal–fullerene bonding.

In the upper panel of Fig. 5, all the WFCs are shown as red spheres. More interesting for our purposes is the distribution of these centers in the region between the metallic Pt atom and the π-66 bond, shown in the lower panel of the same figure. A first feature worthy of note is the isotropic distribution of eight WFCs around the Pt site, all of them mainly coming from a combination of the 5*d* states of Pt. These WFCs close to the Pt atoms are labeled in Fig. 5 according to the order in which they appear after the mentioned unitary transformation. By looking at their associated spread, two groups of centers can be identified. The WFCs labeled as 2, 3, 121, and 129 are characterized by a dispersion $\sigma_{WFC} = 0.78$ Å, whereas WFCs 1, 4, 120, and 127 have a slightly larger spread $\sigma_{WFC} = 0.82$ Å. Additionally, two WFCs with labels 7 and 24 appear to be located at nearly equal distances along the Pt–C bonds. Indeed, the distances between Pt and each one of these two WFCs amount to 1.02 Å, while the distances between the C atoms forming the π-66 bond are 1.03 Å. This is a clear indication that these two

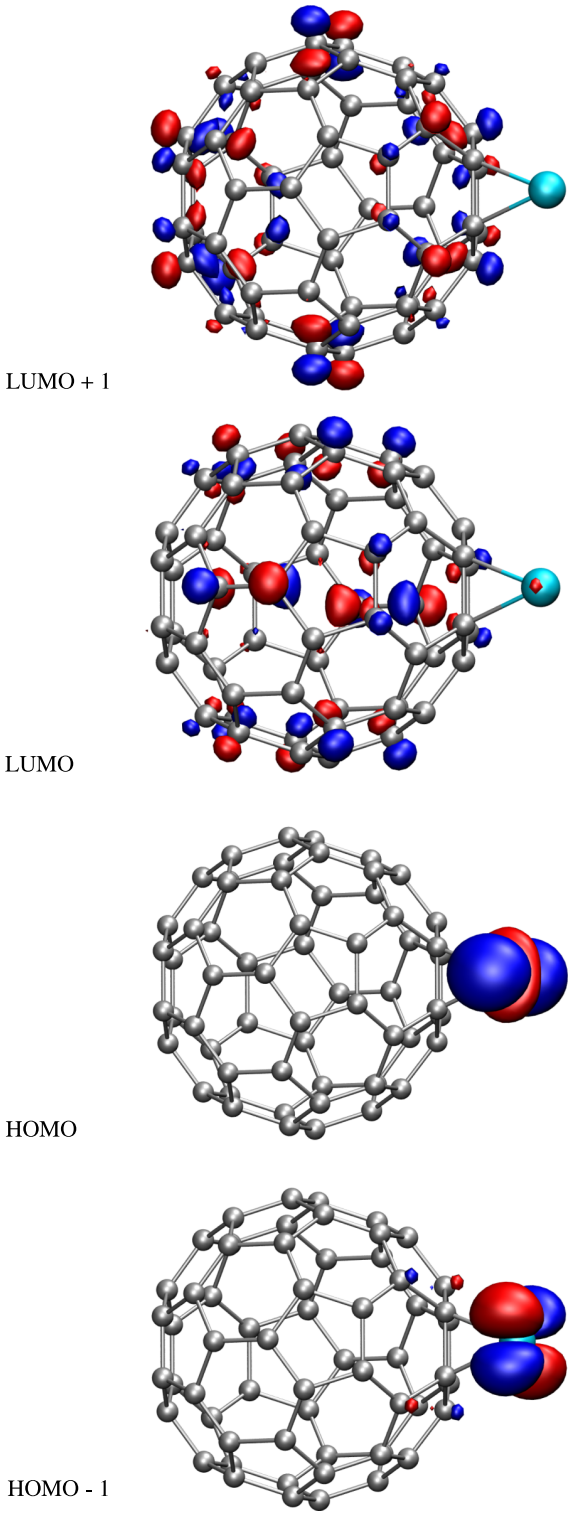

FIG. 4. Wavefunctions of the HOMO-1, HOMO, LUMO and LUMO+1 states of the Pt–C_{60} system. Isosurfaces are shown at values of $\pm 0.05\ (e/\text{Å}^3)^{1/2}$ and the color code is blue for positive amplitudes and red for negative amplitudes.

WFCs account for the bonding between the metal atom and the fullerene. For this same reason, the spread associated to these WFCs is as large as 1.20 Å, and such a large dispersion accounts for the formation of stable metal-carbon bonds of the system. A more explicit view of the Wannier functions corresponding to the WFCs 7 and 24 is shown in Fig. 6, where

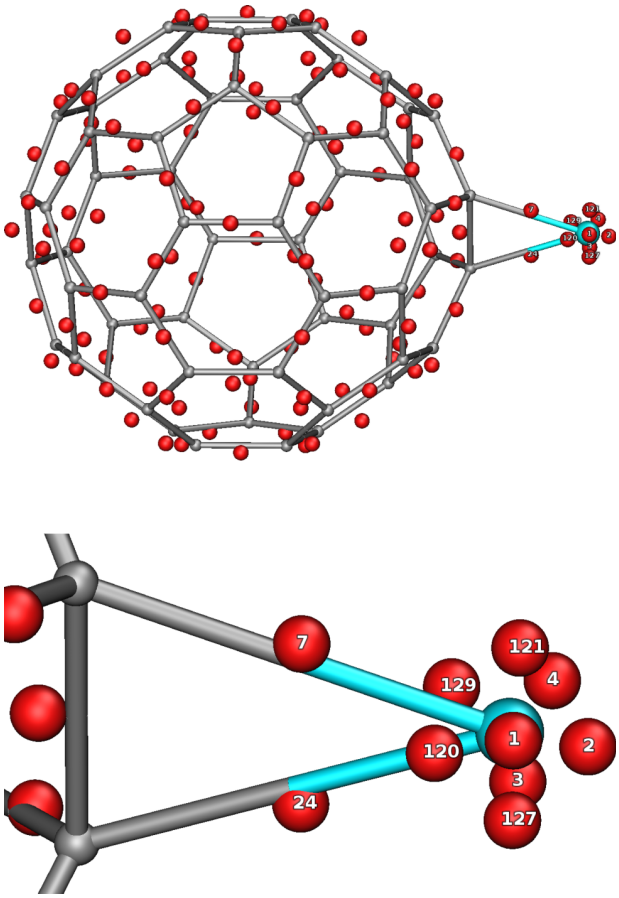

FIG. 5. Wannier centers for the fullerene-Pt complex (upper panel) and detail around the Pt–C_{60} interface (lower panel) where two specific centers, labeled 7 and 24, participate to the metal–C_{60} bonds. Details are discussed in the text.

the isosurface (0.1 eV/Å^3) of the localized orbitals along the Pt–C_{60} π-66 bonds extend over the whole bond length.

Additional information about the Wannier functions around the Pt and Pd metal atoms is shown in the supplementary figures S1 and S2.[47]

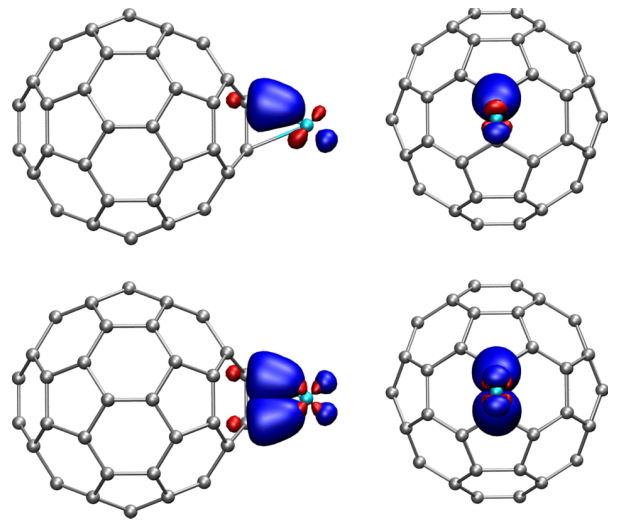

FIG. 6. Maximally localized Wannier functions for the centers involved in the Pt–C_{60} π-66 bond. Isosurfaces are shown at values of $\pm 0.1\ (e/\text{Å}^3)^{1/2}$ with the blue and red colors corresponding to positive and negative values, respectively.

IV. FULLERENE COMPLEXES WITH TWO METAL ATOMS

A. Structural properties

The introduction of a second metal into the system discloses a number of different possibilities concerning the location of the additional atom, on the simple basis of the symmetry of the system. As in the case of the initial configuration of a single metal atom, assuming stable (a) and metastable (b) configurations of the M–C_{60} complex as a starting point, there are eight possible *a priori* scenarios. These are labeled from (a) to (h) and summarized in Fig. 7. Moreover, an additional configuration, identified by label (i), can be included by considering structure (h) after reversing the position of the two metallic atoms, Pt and Pd.

Static structural optimizations followed by dynamics for each one of the configurations labeled from (a) to (h) resulted in the situation summarized in Table III. Namely, the most stable isomer in all cases is the one shown in Fig. 8, in which the metal atoms, regardless of their species, are located on top of two π-66 bond (see left panel of the figure). It is noteworthy to mention that the C atoms bonded to either one of the metals atoms form a four-membered chain of adjacent neighbors along the perimeter of a pentagonal motif of the C_{60}.

When the two metal atoms are both Pt, all the configurations from (b) to (h) are less stable than the (a) configuration by as much as ∼0.2 eV. Interestingly, we did not observe any attempts of the system, neither during the optimization nor during the dynamics, to recover spontaneously the (a) structure. This is clearly due to the more selective choice we carried out when positioning the second Pt always on π-66 sites, an insight issued from the single-metal search for stable locations. Analogously, if both metal atoms are Pd, the configurations labeled from (b) to (g) are energetically above the (a) structure by ∼0.2 eV. A noticeable difference, instead, arises when the two metallic atoms are adjacent as in the (h) configuration. In fact, because of the different nature and equilibrium relative distances of Pt with respect to Pd,[48] the alignment of two Pd atoms on the same side of the fullerene becomes energetically more costly with the resulting metastable system located above the (a) configuration by 0.81 eV. This is a configuration unlikely to be accessible experimentally. Focusing on the case of two different metal atoms, the above energetical pattern is recovered. Indeed, all configurations from (b) to (h) lie above most stable configuration (a) by about 0.3 eV. However, this time the (h) configuration is more accessible, at least if the atom closer to the fullerene is Pt. Conversely, if the order of the metal atoms is reversed, corresponding to the configuration labeled as (i) in Table III, the system is located at much higher energies (1.12 eV).

Focusing on the (a) configurations, which is the ground state, the main geometrical parameters are reported in Table IV. Metal–carbon distances range between 2.1 and 3.8 Å. These relatively large variations are the result of the vicinity of the metal atoms, their mutual repulsion or attraction, and the bond form with the C atoms belonging to the π-66 bonds. The last row of the table shows how the relative distance of the two metallic atoms changes according to the nature of the metals involved. Specifically, Pt atoms have a tendency to stay closer to each other (3.01 Å) than Pd atoms (3.25 Å), while

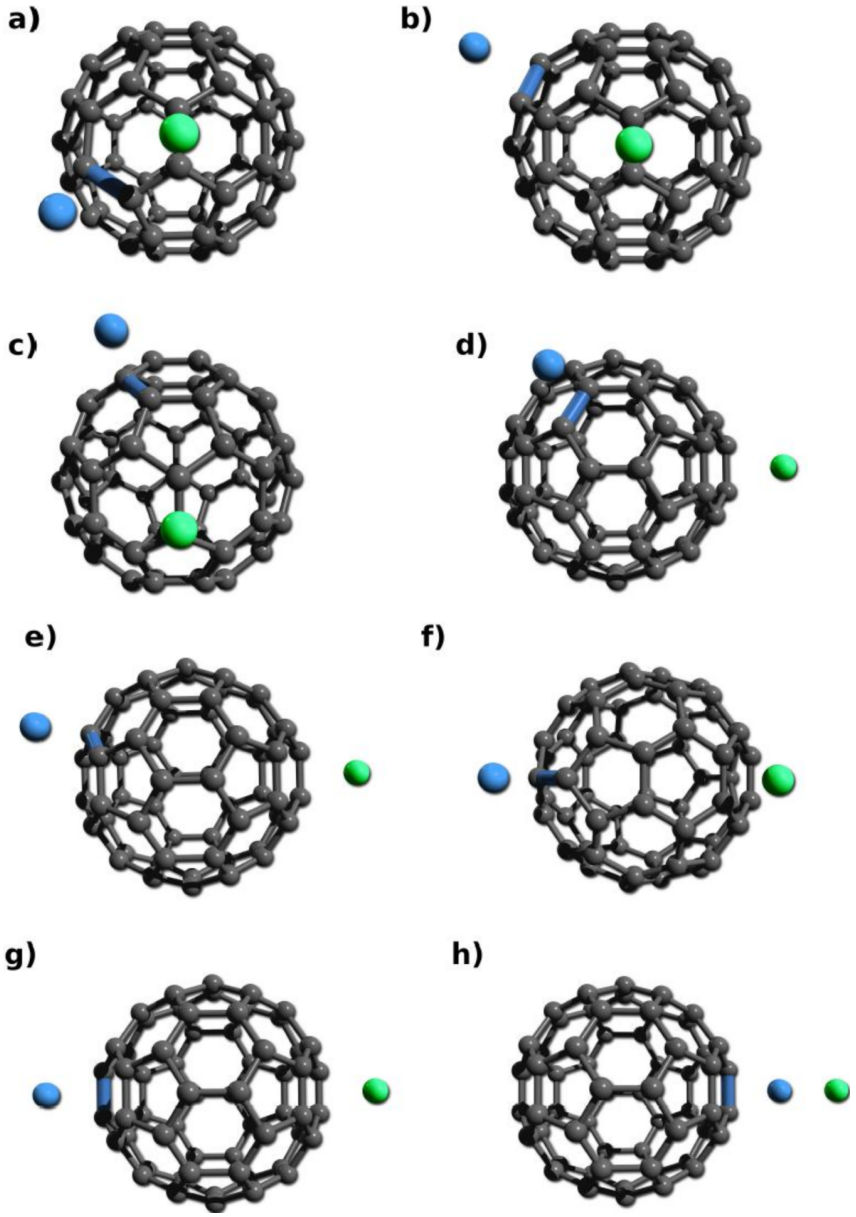

FIG. 7. Schematic representation of the initial configurations for the M_2–C_{60} systems. The first metallic atom (in green) is located on the equilibrium position (on top of a π-66 bond) determined in the M–C_{60} study. Then a second metallic atom (in blue) is added on top of another π-66 bond (between two C_6 rings) highlighted in blue. Using the symmetry properties of C_{60} this leads to a maximum of 8 different initial configurations. From (a) to (g) the distance between the two M atoms increases, (h) the two M atoms are located on top of the same π bond. For $M_1 \neq M_2$ it is possible to define an additional configuration (i) where the order of the positions is inverted.

TABLE III. M_2–C_{60} (M = Pt, Pd) initial and final configurations along with the total energy differences ΔE between the final configuration and the most stable configuration for each system.

	M_2–C_{60}					
	$M_1 = M_2 = Pt$		$M_1 = M_2 = Pd$		$M_1 = Pt \neq M_2 = Pd$	
Initial	Final	ΔE (eV)	Final	ΔE (eV)	Final	ΔE (eV)
a	a	0.0	a	0.0	a	0.0
b	b	0.23	b	0.20	b	0.30
c	c	0.23	c	0.19	c	0.30
d	d	0.17	d	0.18	d	0.27
e	e	0.20	e	0.18	e	0.28
f	f	0.18	f	0.17	f	0.27
g	g	0.20	g	0.18	g	0.29
h	h	0.17	h	0.81	h	0.31
					i	1.12

two closeby different chemical species, Pt and Pd, are the best compromise to minimize the mutual repulsion and bring the two metal sites as close as 2.91 Å.

B. Electronic properties

The addition of a second metal atom to the system results in a further shrinking of the energy gap with respect to both the

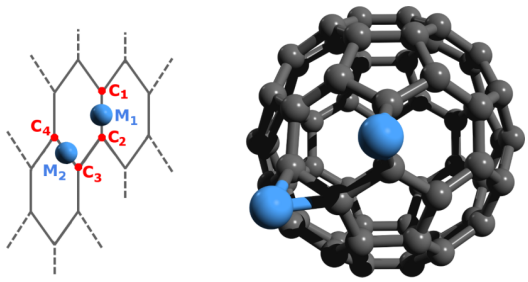

FIG. 8. Schematic (left) and 3D representations (right) of the M_2–C_{60} complex for the most stable isomer (a) (see Fig. 7).

TABLE IV. Final geometry for the most stable M_2–C_{60} (a) configuration. (see Fig. 8). Distances are in Å.

	M_2–C_{60}					
	$M_1 = M_2 = Pt$		$M_1 = M_2 = Pd$		$M_1 = Pt \neq M_2 = Pd$	
	d_{M_1-C}	d_{M_2-C}	d_{M_1-C}	d_{M_2-C}	d_{M_1-C}	d_{M_2-C}
C_1	2.10	3.66	2.21	3.79	2.09	3.61
C_2	2.02	2.95	2.14	3.07	2.03	2.90
C_3	2.94	2.02	3.08	2.13	2.99	2.11
C_4	3.65	2.10	3.80	2.22	3.70	2.31
	d_{Pt-Pt}		d_{Pd-Pd}		d_{Pt-Pd}	
	3.01		3.25		2.91	

bare fullerene[44] and the complex metal–C_{60}. The reason is the appearance of metallic states $5d^9 6s^1$ (Pt) and $4d^{10}$ (Pd) in the energy gap of the C_{60}. More precisely, by the combination of these metallic states into d_{z^2} and $d_{x^2-y^2}$ orbitals, as sketched in Fig. 9. The values of the gap of the M_2–C_{60} systems are 0.95 eV (Pd–Pd), 0.63 eV (Pt–Pd), and 0.48 eV (Pt–Pt). As in the case of single-metal systems, the HOMO states are basically d_{z^2} states centered on the metallic atoms, whereas HOMO-1 levels have a $d_{x^2-y^2}$ character with minor amplitudes extending on the C atoms belonging to the π-66 site on which Pd and/or Pt are located; corresponding wavefunctions are shown in the supplementary figure S3.[47] It can be remarked that the addition of metal atoms is a practical way to construct building blocks metal–C_{60} in which the amplitude of the gap can be tuned as a function of the metal atoms participating to the complex.

Coming to the Wannier centers representation and their associated spread, we can observe that the distribution of WFCs for both atoms resembles closely the one discussed in the case of a single metal atom. By focusing on the two doubly occupied WFCs are located roughly in the middle of the metal–C bonds (see Fig. 10) and characterized by a large spread typical of chemical bonds. Nonetheless, a slight difference can be remarked in the position of the two WFCs.

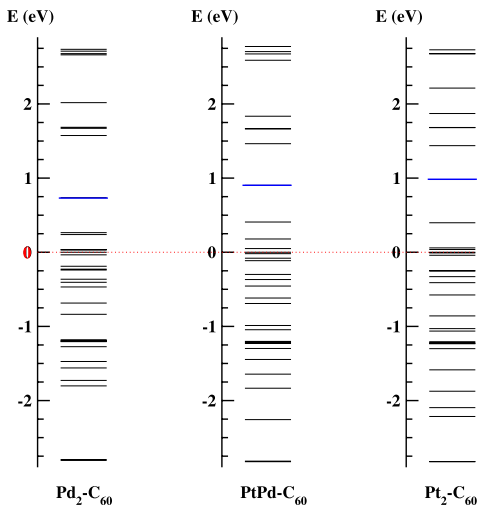

FIG. 9. Band structure for the M_2–C_{60} (M = Pt, Pd) systems. Panels from left to right refer to Pd_2–C_{60}, PtPd–C_{60}, and Pt_2–C_{60}, respectively.

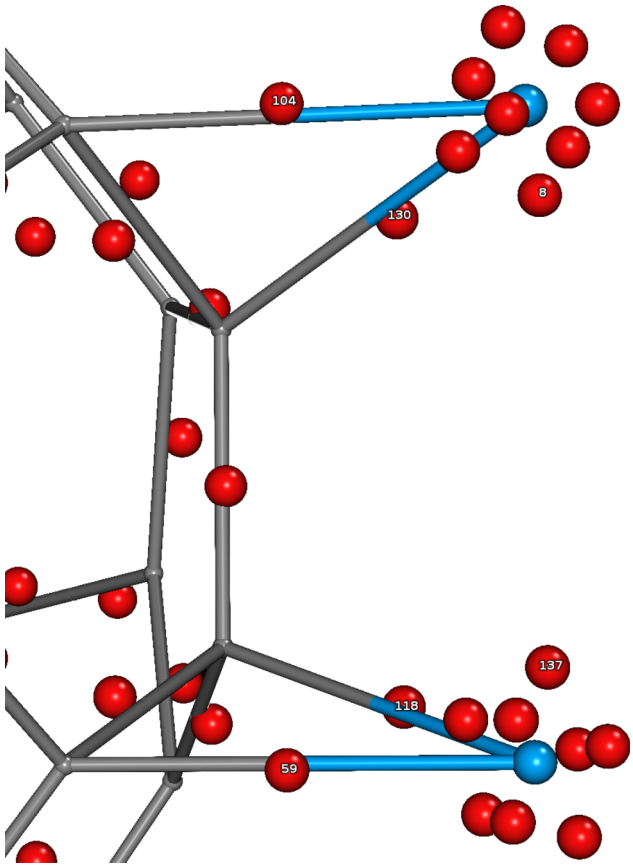

FIG. 10. Positions of the main Wannier functions centers around the Pt_2–C_{60} system.

More precisely, by focusing on the two WFCs labeled as 104 and 130 of Fig. 10, the distances of these two centers from the closest Pt atom are 1.10 and 0.95 Å, respectively. This slight asymmetry is found also for the second Pt atom with respect to the WFCs 59 and 118. As a consequence, the associated spreads for all these four centers amount to 1.23 Å (to be compared with the 1.20 Å found in the case of a single metal atom bound to the C_{60}). The slightly larger spread compensates the small asymmetry and ensures a stable metal–carbon bond as in the single metal case. Equally interesting is the clustering effect of the metals on the fullerene.[39] In fact, by looking at the two WFCs labeled as 8 and 137, corresponding to electronic states facing each other on the two metal sites, we remark that the spread of these two states amounts to 0.97 Å, a value that is peculiar to these two specific sites. In fact, large spreads in M–C_{60} can be found only for WFCs belonging to carbon metal bonds (see Fig. 5 for comparison). This increased value of the spread is an indicator of the tendency of the metal atoms to clusterize on the external surface of the fullerene. Moreover, this allows to infer that the gap tuning process is a delicate issue that cannot be reduced simply to the crude algebraic addition of the results obtained on a single-metal–C_{60} complex. In fact, the approach of WFCs of nearby metal atoms is limited on the one hand by the electrostatic Coulomb repulsion and, on the other hand, by the Pauli repulsion. The subtle combination of these two interactions is responsible, from the structural point of view, for the more or less pronounced approaching of the two metals and, from the electronic point of view, for the

redistribution of the electronic energy levels, hence the gap of the resulting complex.

Complementary information about the global distribution of Wannier centers and Wannier orbitals around the two metal atoms is reported in the supplementary figures S4 and S5.[47]

V. CONCLUSION

Focusing on the use of metallo-fullerene complexes as building blocks for nanostructures prone to have applications in fuel cells, catalysis, and nanoelectronics, we studied how Pt and Pd atoms can be accommodated in a stable way on the external surface of fullerenes. The atomic-scale details of the interaction between a C_{60} with one or two metallic atoms has shown that the high symmetry of the fullerene and the underlying electronic structure favor the formation of Pt and Pd adsorption sites on π-66 bonds. The additional interaction between two metal atoms simultaneously present on the fullerene is the driving force that discriminates between stable and unstable configurations. The nature of the metal-fullerene bonds has been analyzed in detail, showing that the stability of the metal atoms on the π-66 sites is ensured by large spreads of wavefunctions that are formed as a contribution of fullerene delocalized π states and metallic *d*–states (and *s*–states for Pt). From an electronic point of view, the large gap of the fullerene is gradually filled by new electronic states due to the presence of the metals. On a wider perspective, extrapolating the present results to large composite structures, we can infer that the formation of fullerene-metal nanostructures will allow for a gap tuning of the resulting system according to the number of M_2–C_{60} building blocks and their arrangements. Equally important issues for synthesis and applications are the intimate relationships between the gap and the metal–fullerene bond lengths and the clustering effect that metallic atoms display when placed on the C_{60} external surface. This provides an important guideline for the realization of nanostructures possessing an insulating, semiconducting, or even metallic character for future nanoelectronics and nanocatalysis applications.

ACKNOWLEDGMENTS

This work was granted access by GENCI (Grand Equipement National de Calcul Intensif) under allocations DARI Nos. x2015096941, x2015095071, and x2015096092. We are grateful to the Direction Informatique (Pole High Performance Computing, HPC) of the University of Strasbourg for providing generous allocation to computing resources. Part of the HPC resources were funded by the Equipex Equip@Meso project.

[1]S. J. Peighambardoust, S. Rowshanzamir, and M. Amjadi, Int. J. Hydrogen Energy **35**, 9349 (2010).
[2]A. V. Krasheninnikov, P. O. Lehtinen, A. S. Foster, P. Pyykkö, and R. M. Nieminen, Phys. Rev. Lett. **102**, 126807 (2009).
[3]M. Sun, H. Liu, Y. Liu, J. Qu, and J. Li, Nanoscale **7**, 1250 (2015).
[4]S. Okada and A. Oshiyama, Phys. Rev. B **68**, 235402 (2003).
[5]N. Park, M. Yoon, S. Berber, J. Ihm, E. Osawa, and D. Tománek, Phys. Rev. Lett. **91**, 237204 (2003).
[6]A. Rodríguez-Fortea, A. L. Balch, and J. M. Poblet, Chem. Soc. Rev. **40**, 3551 (2011).
[7]A. Rodríguez-Fortea, N. Alegret, A. L. Balcj, and J. M. Poblet, Nat. Chem. **2**, 955 (2010).
[8]K. Toth, J. K. Molloy, M. Matta, B. Heinrich, D. Guillon, G. Bergamini, F. Zerbetto, B. Donnio, P. Ceroni, and D. Felder-Flesch, Angew. Chem., Int. Ed. **52**, 12303 (2013).
[9]D. Felder-Flesh, *Fullerenes and Other Carbon-Rich Nanostructures Structure and Bonding* (Springer-Verlag, Berlin Heidelberg, 2014), Vol. 159, p. 101.
[10]I. M. L. Billas, C. Massobrio, M. Boero, M. Parrinello, W. Branz, F. Tast, N. Malinowski, M. Heinebrodt, and T. P. Martin, Comput. Mater. Sci. **17**, 191 (2000).
[11]M. Matsubara, J. Kortus, J. C. Parlebas, and C. Massobrio, Phys. Rev. Lett. **96**, 155502 (2006).
[12]R. Scipioni, M. Matsubara, E. Ruiz, C. Massobrio, and M. Boero, Chem. Phys. Lett. **510**, 14 (2011).
[13]B.-Y. Sun, Y. Sato, K. Suenaga, T. Okazaki, N. Kishi, T. Sugai, A. Bandow, S. Ijima, and H. Shinohara, J. Am. Chem. Soc. **127**, 17972 (2005).
[14]T. W. Chamberlain, J. C. Meyer, J. Biskupek, J. Leschner, A. Santana, N. A. Besley, E. Bichoutskaia, U. Kaiser, and A. N. Khlobystov, Nat. Chem. **3**, 732 (2011).
[15]G. Krosnicki, "Using fullerenes as catalyst support for proton exchange membrane fuel-cells," Ph.D. thesis, University of Strasbourg, France, 2011, http://scd-theses.u-strasbg.fr/2405/.
[16]W. Andreoni and A. Curioni, Phys. Rev. Lett. **77**, 834 (1996).
[17]K. Prassides, M. Keshavarz, J. C. Hummelen, W. Andreoni, P. Giannozzi, E. Beer, C. Bellavia, L. Cristofolini, R. González, A. Lappas, Y. Murata, M. Malecki, V. Srdanov, and F. Wudl, Science **271**, 1833 (1996).
[18]Y. Rikiishi, Y. Kashino, H. Kusai, Y. Takabayashi, E. Kuwahara, Y. Kubozono, T. Kambe, T. Takenobu, Y. Iwasa, M. Mizorogi, S. Nagase, and S. Okada, Phys. Rev. B **71**, 224118 (2005).
[19]W. Kohn and L. J. Sham, Phys. Rev. **140**, A1133 (1965).
[20]A. D. Becke, Phys. Rev. A **38**, 3098 (1988).
[21]C. Lee, W. Yang, and R. G. Parr, Phys. Rev. B **37**, 785 (1988).
[22]W. Andreoni, Annu. Rev. Phys. Chem. **49**, 405 (1998).
[23]M. Steinmetz and S. Grimme, ChemistryOpen **2**, 115 (2013).
[24]N. Troullier and J. L. Martìns, Phys. Rev. B **43**, 1993 (1991).
[25]R. N. Barnett and U. Landman, Phys. Rev. B **48**, 2081 (1993).
[26]A. A. Scheidemann, V. V. Kresin, and W. D. Knight, Phys. Rev. A **49**, R4293 (1994).
[27]S. Grimme, J. Comput. Chem. **27**, 1787 (2006).
[28]J. Hutter, H. P. Lüthi, and M. Parrinello, Comput. Mater. Sci. **2**, 244 (1993).
[29]M. I. J. Probert, J. Comput. Phys. **191**, 130 (2003).
[30]R. Car and M. Parrinello, Phys. Rev. Lett. **55**, 2471 (1985).
[31]CPMD, Copyright IBM Corp. 1990–2014, Copyright MPI für Festkörperforschung Stuttgart 1997-2001, www.cpmd.org.
[32]N. Marzari and D. Vanderbilt, Phys. Rev. B **56**, 12847 (1997).
[33]R. Resta and S. Sorella, Phys. Rev. Lett. **82**, 370 (1999).
[34]M. Boero, J. Phys. Chem. A **111**, 12248 (2007).
[35]P. L. Silvestrelli, N. Marzari, D. Vanderbilt, and M. Parrinello, Solid State Commun. **107**, 7 (1998).
[36]I. M. L. Billas, C. Massobrio, M. Boero, M. Parrinello, W. Branz, F. Tast, N. Malinowski, M. Heinebrodt, and T. P. Martin, J. Chem. Phys. **111**, 6787 (1999).
[37]M. Boero, M. Parrinello, S. Huffer, and H. Weiss, J. Am. Chem. Soc. **122**, 501 (2000).
[38]F. L. Gervasio, A. Laio, M. Parrinello, and M. Boero, Phys. Rev. Lett. **94**, 158103 (2005).
[39]L. M. Ramaniah, M. Boero, and M. Laghate, Phys. Rev. B **70**, 035411 (2004).
[40]M. Matsubara, C. Massobrio, L. M. Ramaniah, E. Ruiz, and M. Boero, Phys. Rev. B **81**, 195433 (2010).
[41]B. P. Feuston, W. Andreoni, M. Parrinello, and E. Clementi, Phys. Rev. B **44**, 4056 (1991).
[42]S. Saito and A. Oshiyama, Phys. Rev. Lett. **66**, 2637 (1991).
[43]J. Hutter, H. P. Luthi, and M. Parrinello, Comput. Mater. Sci. **2**, 244 (1994).
[44]S. M. Lee, R. J. Nicholls, D. Nguyen-Manh, D. G. Pettifor, G. A. D. Briggs, S. Lazar, D. A. Pankhurst, and D. J. H. Cockayne, Chem. Phys. Lett. **404**, 206 (2005).
[45]K. Morokuma and W. T. Borden, J. Am. Chem. Soc. **113**, 1912 (1991).
[46]Q. Zhou, S. Coh, M. L. Cohen, S. G. Louie, and A. Zettl, Phys. Rev. B **88**, 235431 (2013).
[47]See supplementary material at http://dx.doi.org/10.1063/1.4930264 for Wannier functions localized around metal sites and HOMO–LUMO states for the case of two metal atoms.
[48]G. W. Graham, P. J. Schmitz, and P. A. Thiel, Phys. Rev. B **41**, 3353 (1990).